Thermodynamics of chaotic relaxation processes

Domenico Lippolis[*]

Institute for Applied Systems Analysis, Jiangsu University, Zhenjiang 212013, China

(Dated: April 16, 2024)

The established thermodynamic formalism of chaotic dynamics, valid at statistical equilibrium, is here generalized to systems out of equilibrium, that have yet to relax to a steady state. A relation between information, escape rate, and the phase-space average of an integrated observable (e.g. Lyapunov exponent, diffusion coefficient) is obtained for finite time. Most notably, the thermodynamic treatment may predict the finite-time distributions of any integrated observable from the leading and subleading eigenfunctions of the Perron-Frobenius/Koopman transfer operator. Examples of that equivalence are shown, and the theory is tested numerically in three paradigms of chaos.

I. INTRODUCTION

The exponential stretching and folding of phase-space densities that characterizes chaotic dynamics makes long-time evolution unpredictable, and with that the problem of motion intractable. It is then customary to study the statistical properties of the phase space, and in particular to aim at estimating long-time expectation values of relevant observables, under the assumption of asymptotic relaxation of the system to an equilibrium- or a steady state.

In this framework finds its roots the thermodynamic formalism [1–4], developed from the 1970s on, that is based on the idea of using large-deviation theory to define a dynamical analog of the thermodynamic Gibbs states, which, at statistical equilibrium, do maximize the generating functional of the desired averages, their fluctuations, and multitime correlation functions. This approach is at the basis of the formulation of evolution operators and periodic orbit theory [5], and it has more recently been employed to elucidate the relation between Lyapunov exponents and decay of correlations [6], as well as to identify dynamical phase transitions in deterministic chaos [7].

This paper aims at extending the thermodynamic formalism of chaotic dynamics to out-of-equilibrium systems. The Gibbs states of the original formulation are here generalized to include time-dependent weights, later identified with phase-space densities transported by the transfer operator (Perron-Frobenius or Koopman) that governs the time evolution of the system. The so-surmised probabilities for the dynamical microstates give rise to a time-dependent free energy ('topological pressure'), that is related not only to the finite-time dynamical averages of interest to us, but crucially, to the entire phase-space distributions of the relevant observables.

In the remainder of the present section, I will concisely review the fundamentals and the main results of the thermodynamic formalism of chaotic systems at statistical equilibrium. In section II, I shall extend the key definition of Gibbs probability for an integrated observable on a chaotic trajectory to a system that has yet to reach equilibrium. Consequently, I derive an expression for finite time, which relates escape rate and Rényi information with free energy ('topological pressure') and a newly introduced quantity named tilted information. This non-equilibrium first law approaches the renowned Kantz-Grassberger relation [8] as the system relaxes to equilibrium or steady state. Section III contains the main implications of the out-of-equilibrium thermodynamic formalism: the profile of the phase-space distribution of any integrated observable at finite time is expressed in terms of the Perron-Frobenius- or Koopman spectrum. The time-dependent field distributions are so estimated in terms of the first two eigenfunctions in a way that does not depend on the choice of the observable. These claims are numerically validated on two paradigmatic models of chaos, namely the perturbed cat map (sec. IV A), a hyperbolic system defined on a torus, which has no escape and whose transient dynamics is entirely ruled by the second eigenfunction of the transfer operators, and the Hamiltonian Hénon map (sec. IV B) with weak additive noise, whose dynamics is essentially governed by a chaotic saddle, but it also features an isolated, marginally stable fixed point, which hinders hyperbolic behavior locally.

While the dependence of the out-of-equilibrium observable distributions on the first two eigenfunctions of the transport operator is general, the universality of their profiles breaks down when squeezing is introduced. It is the case of strange attractors, where time-dependent field distributions are found to be observable specific. This is exemplified in sec. IV C by the noisy Ikeda attractor.

A. Gibbs states

In the thermodynamics of equilibrium, the entropy S is maximal when the internal energy E is fixed (microcanonical ensemble), while the free energy F is minimized when the internal energy fluctuates (canonical ensemble)

$$F = E - k_B T\, S \,. \tag{1}$$

---
[*] domenico@ujs.edu.cn

The Gibbs (canonical) ensemble is made of a number of subsystems, each occurring with a probability p_j:

$$E = \sum_j p_j E_j \tag{2}$$

$$S = -\sum_j p_j \ln p_j, \tag{3}$$

so that $(\beta = 1/k_B T)$

$$F = \sum_j p_j E_j + \frac{1}{\beta} \sum_j p_j \ln p_j. \tag{4}$$

Using Calculus, one can show that the free energy is minimized by choosing

$$P_j = \frac{e^{-\beta E_j}}{\sum_i e^{-\beta E_i}}. \tag{5}$$

P_j is the probability of the subsystem labelled by j to have energy E_j. At equilibrium,

$$F_{\min} = -\ln \sum_i e^{-\beta E_i}. \tag{6}$$

The Gibbs formalism has been used to describe chaotic dynamics of ergodic and mixing systems, which, in general do not reach thermodynamic-, but rather statistical equilibrium, asymptotically. Here goes a summary of how that works.

B. Thermodynamics of chaos

The analysis that follows is formulated for low-dimensional chaotic systems, such as expanding maps on the interval, or hyperbolic Axiom A systems, such as the cat map, whose phase space may be partitioned to a number of distinct regions, and trajectories can be encoded with symbolic sequences [5], tracking the regions visited by each orbit at every instant. In the thermodynamical picture of chaotic dynamics, the phase space is the whole (canonical) ensemble, whose subsystems/Gibbs states are identified with the single (ergodic) trajectories, the latter thought of as infinite sequences in the long-time limit.

In the formalism, the Boltzmann constant β becomes a parameter: given the map $x_{n+1} = f(x_n)$, that defines the dynamics, identify the energy with the integrated observable

$$E_j(t) = A_j^t = \int_0^t a\left[f^\tau(x_0)\right] d\tau, \tag{7}$$

where j tags the symbolic sequence of the trajectory that starts at x_0 and is iterated by τ times by f, and a is in general a function of an operator, for example the differential, in the evaluation of the Lyapunov exponents, or the squared position to yield the diffusion constant as the integrated observable (7). Assuming that the system

reaches equilibrium (or a stationary state) for $t \to \infty$, it has been proven [1, 2] that the Gibbs probabilities

$$p_j(t) = \frac{e^{-\beta E_j(t)}}{\sum_i e^{-\beta E_i(t)}} \tag{8}$$

minimize the 'free energy', or equivalently, maximize the quantity

$$\mathcal{P}(\beta) = \lim_{t \to \infty} \frac{1}{t} \ln \sum_j e^{-\beta E_j(t)}, \tag{9}$$

that is known as 'topological pressure' [9], although it is in fact a free energy. It has been shown that Eqs. (8)-(9) imply the relation

$$\mathcal{P}(\beta) = \langle A \rangle_\beta + h_\beta, \tag{10}$$

analogous to Eq. (1) for the free energy, where $\langle \cdot \rangle$ denotes an ensemble average, and

$$h_\beta = -\lim_{t \to \infty} \frac{1}{t} \frac{1}{\beta - 1} \ln \sum_i^r p_i^\beta(t) \tag{11}$$

is called Rényi entropy. Equation (10) becomes more familiar when $\beta = 1$, and $\langle A \rangle$ is the positive Lyapunov exponent of the dynamics. In that case, $\mathcal{P}(1)$ is (minus) the escape rate γ_0, while

$$h_1 = -\lim_{t \to \infty} \frac{1}{t} \sum_i^r p_i(t) \ln p_i(t) \tag{12}$$

is the information entropy. One can then write (10) as [3, 8, 10]

$$h_1 = -\gamma_0 + \lambda, \tag{13}$$

that relates information entropy, escape rate, and Lyapunov exponent λ.

II. FINITE-TIME THERMODYNAMICS

Let us attempt to extend the thermodynamic formalism to finite time, out of equilibrium. I shall begin with a finite-time topological pressure, of the type

$$\mathcal{P}_t(\beta) = \frac{1}{t} \ln \sum_j w_j(t) e^{-\beta A_j^t}, \tag{14}$$

which, technically, may no longer be considered a free energy, since we are now out of equilibrium. The factors w_j are included in the previous expression for the topological pressure, so that the Gibbs probabilities for every trajectory throughout the Markov partition are now weighted:

$$p_j(t) = \frac{w_j(t) e^{-\beta A_j^t}}{\sum_i w_i(t) e^{-\beta A_i^t}}. \tag{15}$$

At this stage, the previous expression is an Ansatz for the probability of the integrated observable to be A_j^t in the subsystem (i.e. symbolic sequence) labelled by j, surmised consistently with the tilted probability (large-deviations) formalism in a dynamics context [11, 12]. The meaning of Eq. (15) will become clearer later on in this section, when the weights $w_j(t)$ are recognized as phase-space densities transported by the dynamics via the Perron-Frobenius/Koopman operator.

In what follows, I distinguish β, inverse temperature, or more simply variable of the charac-

teristic (moment-generating, partition-) function $Z_t(\beta) = \sum_j w_j(t)e^{-\beta\,A_j(t)}$, from q, order of the Rényi entropy, and I use the so-generalized expression for the topological pressure

$$\mathcal{P}_t(q,\beta) = \frac{1}{t}\ln\sum_j w_j^q(t)e^{-q\beta\,A_j^t}\,, \qquad (16)$$

whereas it is still understood that $\mathcal{P}_t(\beta) := \mathcal{P}_t(q=1,\beta)$. The Rényi information is the entropy (11) for finite time:

$$I_t(q,\beta) = -\frac{1}{t}\frac{1}{q-1}\ln\sum_i^r p_i^q(t) = \frac{1}{1-q}\frac{1}{t}\ln\sum_j \frac{w_j^q e^{-q\beta\,A_j^t}}{\left[\sum_i w_i e^{-\beta A_i^t}\right]^q}$$

$$= \frac{1}{1-q}\frac{1}{t}\ln\frac{e^{\mathcal{P}_t(q,\beta)t}}{Z_t^q(\beta)} = \frac{1}{1-q}\left[\mathcal{P}_t(q,\beta) - \frac{1}{t}\ln Z_t^q(\beta)\right]\,. \qquad (17)$$

The previous can be rewritten as

$$I_t(q,\beta) = \frac{1}{1-q}\left[\mathcal{P}_t(q,\beta) - q\,\mathcal{P}_t(\beta)\right]\,, \qquad (18)$$

keeping in mind that everything is time dependent, and out of equilibrium. In the limit $q \to 1$, we have that

$$I_t(1,\beta) = \mathcal{P}_t(\beta) - \mathcal{P}_t'(\beta) = \frac{1}{t}\left[\ln\sum_j w_j e^{-\beta\,A_j^t} - \frac{d}{dq}\ln\sum_j w_j^q e^{-q\beta\,A_j^t}\bigg|_{q=1}\right]\,, \qquad (19)$$

where

$$\frac{d}{dq}\ln\sum_j w_j^q e^{-q\beta\,A_j^t}\bigg|_{q=1} = \frac{\sum_j w_j e^{-\beta\,A_j^t}\left[\ln w_j - \beta A_j^t\right]}{Z_t(\beta)}\,. \qquad (20)$$

We can already spot three terms in the right-hand side of Eq. (19). The first is simply $\mathcal{P}_t(\beta)$ with the new definition of weighted probabilities for the symbolic sequences. Let us identify the remaining two terms.

$$\frac{1}{t}\frac{\sum_j \beta A_j^t w_j e^{-\beta\,A_j^t}}{\sum_j w_j e^{-\beta\,A_j^t}} = \frac{1}{t}\frac{\sum_j \beta p_j(t) A_j^t}{\sum_j p_j(t)} = \beta\langle A^t\rangle_\beta\,, \qquad (21)$$

where the average is taken with respect to the definition (15) of the time-dependent probabilities. In that sense, the previous is a thermodynamic average. Unlike in the equilibrium treatment, the entropy-energy-free'energy relation features an extra term, that is

$$\frac{\frac{1}{t}\sum_j w_j \ln w_j\, e^{-\beta\,A_j^t}}{\sum_j w_j e^{-\beta\,A_j^t}} \equiv \frac{S_t(\beta)}{Z_t(\beta)}\,, \qquad (22)$$

and I name the numerator $S_t(\beta)$ *tilted information*. Now Eq. (19) takes the form

$$I_t(1,\beta) = \mathcal{P}_t(\beta) + \beta\langle A^t\rangle_\beta - \frac{S_t(\beta)}{Z_t(\beta)}\,. \qquad (23)$$

Now, as a necessary condition for this theory to make sense, we have to retrieve Eq. (10) from the limit $t \to \infty$ of Eq. (23). An argument may be used from Reference [2] to help determine the asymptotic behavior of our finite-time thermodynamic relation connecting Shannon information, Gibbs average, and topological pressure. Take as integrated observable the finite-time Lyapunov exponent

$$A^t = \ln||J^t(x_0)|| = \ln|\Lambda(t)|\,, \qquad (24)$$

where the Jacobian is defined as

$$J_{ij}^t(x) = \frac{\partial f_i^t(x)}{\partial x_j}\,. \qquad (25)$$

Consider the partition function

$$Z_t(\beta) = -\sum_j \frac{w_j(t)}{|\Lambda_j(t)|^\beta} \,. \qquad (26)$$

Assume that all the weights w_j are bounded by positive constants c_1, and c_2 as

$$c_1 \le w_j \le c_2 \,, \qquad (27)$$

which stands to reason, if the map in question is expanding or hyperbolic, since in that case the dynamics is everywhere unstable and no trajectory/sequence may ever carry infinite statistical weight. We may then sandwich the partition function (26) as

$$c_1 \sum_j \frac{1}{|\Lambda_j(t)|^\beta} \le \sum_j \frac{w_j(t)}{|\Lambda_j(t)|^\beta} \le c_2 \sum_j \frac{1}{|\Lambda_j(t)|^\beta} \,, \qquad (28)$$

and hence

$$\frac{1}{t} \ln c_1 \sum_j \frac{1}{|\Lambda_j(t)|^\beta} \le \frac{1}{t} \ln \sum_j \frac{w_j(t)}{|\Lambda_j(t)|^\beta} \le \frac{1}{t} \ln c_2 \sum_j \frac{1}{|\Lambda_j(t)|^\beta}$$

$$\frac{1}{t} \ln c_1 + \frac{1}{t} \ln \sum_j \frac{1}{|\Lambda_j(t)|^\beta} \le \frac{1}{t} \ln \sum_j \frac{w_j(t)}{|\Lambda_j(t)|^\beta} \le \frac{1}{t} \ln c_2 + \frac{1}{t} \ln \sum_j \frac{1}{|\Lambda_j(t)|^\beta} \,, \qquad (29)$$

so that, when $t \to \infty$, both inequalities saturate to yield the same expression

$$\lim_{t\to\infty} \frac{1}{t} \ln \sum_j \frac{1}{|\Lambda_j(t)|^\beta} = \mathcal{P}(\beta) \,, \qquad (30)$$

that is the topological pressure defined at equilibrium with the unweighted Gibbs probabilities, whose ensemble constitutes the pointwise natural measure of the dynamical system at hand [3]. Besides retrieving $\mathcal{P}(\beta)$ from the $t \to \infty$ limit of $\mathcal{P}_t(1, \beta)$, the previous analysis tells us that the quantity $Z_t(\beta)$ given by Eq. (26) is also bounded as, say, $c_1' \le Z_t(\beta) \le c_2'$.

Let us now apply the same idea as in (28) to the tilted information $S_t(\beta)$: let

$$\chi_1 \le w_j \ln w_j \le \chi_2 \,, \qquad (31)$$

for some χ_1, χ_2, and so

$$\chi_1 \sum_j \frac{1}{|\Lambda_j(t)|^\beta} \le \sum_j \frac{w_j(t) \ln w_j(t)}{|\Lambda_j(t)|^\beta} \le \chi_2 \sum_j \frac{1}{|\Lambda_j(t)|^\beta} \,, \qquad (32)$$

that also results in upper and lower bounds for $t\, S_t(\beta)$. Then we may also sandwich the ratio $t\, S_t(\beta)/Z_t(\beta)$ we have encountered in Eq. (23):

$$\frac{\chi_1'}{c_2'} \le \frac{\sum_j \frac{w_j(t) \ln w_j(t)}{|\Lambda_j(t)|^\beta}}{\sum_j \frac{w_j(t)}{|\Lambda_j(t)|^\beta}} \le \frac{\chi_2'}{c_1'} \,, \qquad (33)$$

with the assumption that $w_j(t) > 0$. The previous bounds are constant in time, and thus, including the fractor of $1/t$ originally in Eq. (23), we have that

$$\lim_{t\to\infty} \frac{S_t(\beta)}{Z_t(\beta)} = \lim_{t\to\infty} \frac{1}{t} \frac{\sum_j \frac{w_j(t) \ln w_j(t)}{|\Lambda_j(t)|^\beta}}{\sum_j \frac{w_j(t)}{|\Lambda_j(t)|^\beta}} = 0 \,, \qquad (34)$$

and Eq. (23) does reduce to the steady-state thermodynamic relation (13) linking information entropy, Lyapunov exponent, and escape rate (for $\beta = 1$).

Let us now identify the weights w_j. The regions of a given partition are evolved by the dynamics, in such a way that the total probability (measure) is conserved at every time step:

$$p_j(t) = \sum_i p_i(t+1) \,. \qquad (35)$$

Using our hypothesis (15) for the p_i's, the previous identity would translate to the evolution

$$\frac{w_j(t)}{|\Lambda_j(t)|^\beta} = e^{-\mathcal{P}_t(\beta)} \sum_i \frac{w_i(t+1)}{|\Lambda_i(t+1)|^\beta} \,, \qquad (36)$$

once we write the probability of every partition element in terms of the stability exponent as integrated observable [Eq. (24)]. This evolution can be written in terms of the Perron-Frobenius operator [6], where we consider the w_j's as densities. For a one-dimensional map, that reads

$$\rho'(x_j) = e^{-\mathcal{P}_t(\beta)} \sum_i \frac{\rho(x_i)}{|f'(x_i)|^\beta} \,. \qquad (37)$$

That identifies the $w_j(t)$'s with time-varying densities.

Now, look at Eq. (36): going from time t to time $t + 1$ means to extend every interval of a Markov partition by one symbol. For instance, if the symbolic dynamics is binary, that is the phase space is partitioned into two regions coded by 0 and 1, we let $t = 3$ and, say, $j = 001$, then $t + 1 = 4$ and the terms of the summation on the right-hand side are $i = 0010, 0011$. In that case, the densities w_j's map forward as stated by the 'Perron-Frobenius' equation (36). If we decide to stop at some definite t and identify the set of all the distinct trajectories with a Markov partition, the p_j's are given by the thermodynamic expression (15), where the w_j's are the densities in each interval of the partition. Therefore, the w_j's are the probabilities of the dynamics to visit each region of the partition, or, equivalently, the probabilities of each trajectory, whereas the p_j's are the probabilities for region (sequence) j to measure the observable A_j^t, and, for finite time, they ought to be weighted by w_j, even if the dynamical system f is ergodic and mixing.

Remarks are in order about the finite-time average and topological pressure. First, for $A^t = \ln |\Lambda(t)|$, the finite-time thermodynamic average (21) becomes

$$\langle \ln |\Lambda(t)| \rangle_\beta = \frac{\sum_j w_j(t) \ln \Lambda_j(t)/\Lambda_j^\beta(t)}{\sum_j w_j(t)/\Lambda_j^\beta(t)}, \qquad (38)$$

which makes sense dynamically, if we recall that the neighborood of each region of a Markov partition of t regions scales as $1/|\Lambda_j(t)|^d$ in a hyperbolic system [3]. That way, Eq. (38) may be regarded as a weighted average over the partition.

On the other hand, the finite-time topological pressure may be reconnected to more familiar quantities such as the moment-generating function in a continuous phase space, where it is written as

$$\begin{aligned} \mathcal{P}_t(\beta) &= \frac{1}{t} \ln \sum_j w_j(t) e^{-\beta A_j^t} \\ &\to \frac{1}{t} \ln \int dx\, w(x(t)) e^{-\beta A^t(x)} = \frac{1}{t} \ln \langle e^{-\beta A^t} \rangle \end{aligned} \quad (39)$$

where the first identity holds in the limit of an infinitely fine partition, with every point in the phase space belonging to a distinct sequence of t symbols, while the derivatives of $\langle e^{-\beta A^t} \rangle$ with respect to β are the moments of the observable A^t weighted by $w(x(t))$ [5]. One may then rewrite Eq. (23) as

$$I_t(1, \beta) = \frac{1}{t} \ln \langle e^{-\beta A} \rangle + \beta \langle A(t) \rangle_\beta - \frac{S_t(\beta)}{Z_t(\beta)}, \qquad (40)$$

recalling that $I_1(\beta)$ and the last two terms do carry a prefactor of $1/t$ in their definitions.

Expressing the probability weights w as phase-space densities in the continuum limit is central in the evaluation of the finite-time averages of the integrated observables and their field distributions, as exposed in what follows.

III.   AVERAGES

In this finite-time thermodynamic picture, an average is taken as in Eq. (21), with the numerator of that expression being

$$\sum_j A_j^t w_j e^{-\beta A_j^t}. \qquad (41)$$

The index j refers to a particular orbit, identified with a symbolic sequence, and thus to a family of trajectories that share the same itinerary throughout the partition up to time t. First, recall the definition (7),

$$A^t(x) = \int_0^t a\left[f^\tau(x)\right] d\tau. \qquad (42)$$

For a long sequence in a Markov partition, I shall approximate the sum over sequences with an integral over the phase space, as seen in Eq. (39). In the phase-space analog of Eq. (41), I can either choose w to be computed at $t = 0$, or at a later t. In the former case, the average may be written

$$\int dx\, A^t(x) w(x) e^{-\beta A^t(x)}, \qquad (43)$$

whereas in the latter, the integrated observable follows the family of trajectories $f^{-t}(x) \to x$ [13], so that

$$\int dx\, A^t(f^{-t}(x)) e^{-\beta A^t(f^{-t}(x))} \left[\mathcal{L}_t w\right](x), \qquad (44)$$

where the Perron-Frobenius evolution operator acts as

$$\begin{aligned} \left(\mathcal{L}_t \cdot w\right)(x) &= \int dy\, \delta(x - f^t(y)) w(y) = \\ &= \sum_{x_0 = f^{-t}(x)} \frac{w(x_0)}{|\det J^t(x_0)|}. \end{aligned} \quad (45)$$

A.   Going forward

Let us first study the average with the weight function evaluated at time t, as in Eq. (44), while Eq. (43) with the density evaluated at time zero will be considered in sec. III C. Assuming a discrete spectrum for the Perron-Frobenius operator, the goal is now to express the average

$$\langle A^t \rangle_\beta = \frac{\int dx\, A^t(f^{-t}(x)) e^{-\beta A^t(f^{-t}(x))} \left[\mathcal{L}_t w\right](x)}{\int dx\, e^{-\beta A^t(f^{-t}(x))} \left[\mathcal{L}_t w\right](x)} \qquad (46)$$

in terms of the leading eigenfunctions of $\mathcal{L}^t$.

In Eq. (44) I now expand $\mathcal{L}_t w$, obtaining

$$\int dx\, A^t(f^{-t}(x))e^{-\beta A^t(f^{-t}(x))}\left[\mathcal{L}_t w\right](x) = \sum_n^\infty b_n e^{-\gamma_n t}\int dx\, \phi_n(x)A^t(f^{-t}(x))e^{-\beta A^t(f^{-t}(x))}, \tag{47}$$

where $e^{-\gamma_n t}$ and $\phi_n(x)$ are respectively eigenvalues and eigenfunctions of the Perron-Frobenius operator $\mathcal{L}_t$, while

$$b_n = \int w(y)\varphi_n(y)dy \tag{48}$$

are the coefficients of the expansion, that depend on the initial densities $w(x)$ and the eigenfunctions φ_n of the Koopman operator $\mathcal{L}_t^\dagger$. Let us then go back to the original thermodynamic average (46), and rewrite it harnessing the above expansion:

$$\langle A^t\rangle_\beta = \frac{\sum_n^\infty b_n e^{-\gamma_n t}\int dx\, \phi_n(x)A^t(f^{-t}(x))e^{-\beta A^t(f^{-t}(x))}}{\sum_n^\infty b_n e^{-\gamma_n t}\int dx\, \phi_n(x)e^{-\beta A^t(f^{-t}(x))}}. \tag{49}$$

Now let $\beta = 0$:

$$\langle A^t\rangle_{\beta=0} = \frac{\sum_n^\infty b_n e^{-\gamma_n t}\int dx\, \phi_n(x)A^t(f^{-t}(x))}{\sum_n^\infty b_n e^{-\gamma_n t}\int dx\, \phi_n(x)}. \tag{50}$$

It is the expansion of an average, and perhaps that does not say much per se. However, we may also turn it into a distribution, if we start with an initial density of the type $w(y) = \delta(y - x_0)$, that is concentrated in one point:

$$\langle A^t\rangle_{\beta=0}(x_0) = \frac{\int dx\, A^t(f^{-t}(x))\int dy\, \delta(x - f^t(y))\delta(y - x_0)}{\int dx\int dy\, \delta(x - f^t(y))\delta(y - x_0)} = \frac{A^t(x_0)}{\mu(\mathcal{M}(t))} =: \hat{A}^t(x_0), \tag{51}$$

where $\mu(\mathcal{M}(t))$ is the fraction of trajectories that do not escape after time t, and it equals unity for a closed system. Concerning the expansion (49), the coefficients b_n defined by Eq. (48) simply equal $\varphi_n(x_0)$ when $w(x) = \delta(x - x_0)$, and the integrated observable spells

$$\langle A^t\rangle_{\beta=0}(x_0) = \hat{A}^t(x_0) = \frac{\sum_n^\infty \varphi_n(x_0)e^{-\gamma_n t}\int dx\, \phi_n(x)A^t(f^{-t}(x))}{\sum_n^\infty \varphi_n(x_0)e^{-\gamma_n t}\int dx\, \phi_n(x)}. \tag{52}$$

In the limit $t \to \infty$, only the first term survives

$$\langle A^t\rangle_{\beta=0}(x_0) \to \frac{\int dx\, \phi_0(x)A^t(f^{-t}(x))}{\int dx\, \phi_0(x)}, \tag{53}$$

that is simply the phase-space average weighted by the invariant density $\phi_0(x)$, as it is known at equilibrium, and the dependence on x_0 has been lost. The interesting time scale in the present context is rather that of $(\gamma_1 - \gamma_0)^{-1}$, at which the expanded average (52) is approximately

$$\hat{A}^t(x_0) := \langle A^t\rangle_{\beta=0}(x_0) \simeq \int_\mathcal{M} A^t(f^{-t}(x))\phi_0(x)\, dx + \frac{\varphi_1(x_0)}{\varphi_0(x_0)}e^{-(\gamma_1-\gamma_0)t}\int_\mathcal{M} A^t(f^{-t}(x))\phi_1(x)\, dx. \tag{54}$$

Now assume that the system has no escape. We may take the natural measure $\phi_0(x)$ to be L^1-normalized in the phase space, while the other eigenfunctions of the Perron-Frobenius operator are such that $\int dx\, \phi_n(x) = 0$. That way, the previous expression for the 'pointwise average' becomes

$$\hat{A}^t(x_0) \simeq \langle A^t\rangle_\mathcal{M} + \varphi_1(x_0)e^{-\gamma_1 t}\int dx\, \phi_1(x)A^t(f^{-t}(x)), \tag{55}$$

where $\langle A^t\rangle_\mathcal{M} = \int dx\, \phi_0(x)A^t(f^{-t}(x))$. In case of no escape ($\gamma_0 = 0$), the ground state of the Koopman operator is a uniform distribution, since

$$\mathcal{L}_t^\dagger \varphi_0(x) = \varphi_0(f^t(x)) = \varphi_0(x) \tag{56}$$

for every x, whence $\varphi_0(x) = 1$ in Eq. (55).

Equation (55) tells us that the distribution of the integrated observable A^t on the phase space is entirely ruled by the subleading eigenfunction $\varphi_1(x)$ of the Koopman

operator at the time scale $1/\gamma_1$, which determines the profile of the distribution $\hat{A}^t(x_0)$ independently of the observable itself.

meaning that the the Koopman operator is supported on the preimage of the set $\mathcal{M}$, and thus $\mathcal{L}_t^\dagger$ may be thought of as transporting a density supported on $\mathcal{M}$ backward in time to a density supported on $f^{-t}(\mathcal{M})$.

B. Perron-Frobenius vs. Koopman operator

The Perron-Frobenius operator $\mathcal{L}_t$ carries a density ρ, supported on $\mathcal{M}$, forward in time to a density supported on a subset of $f^t(\mathcal{M})$ [14]. In this sense, $\mathcal{L}_t$ 'follows the flow'. One the other hand, the Koopman operator $\mathcal{L}_t^\dagger$ acts as

$$\mathcal{L}_t^\dagger \rho(x) = \rho(f^t(x)), \tag{57}$$

and so

$$\rho(f^t(x)) = 0 \qquad \text{if } f^t(x) \notin \mathcal{M}. \tag{58}$$

That implies that

$$\mathcal{L}_t^\dagger \rho(x) = 0 \qquad \text{if } x \notin f^{-t}(\mathcal{M}), \tag{59}$$

C. Going backward : a matter of pinning

But why is the field profile of the integrated observable A^t governed by the eigenfunctions of the Koopman operator, and not by those of its adjoint, the Perron-Frobenius operator? The reason is that in Eq. (44) x is the final point of the density w and of the integrated observable A^t. If, on the contrary, I had chosen to pinpoint density and observable by their values at the initial point of the trajectory originally labelled by the symbolic sequence j in the discretized state space, I could have written w as an evolution by the Koopman operator:

$$w(f^t(x)) = \int dy\, \delta(y - f^t(x)) w(y). \tag{60}$$

Then, the course of action leading to the expansion of the average (49) is 'adjointed'. Let us use the definition (42) for the integrated observable as a function of x_0, that is the initial point, and rewrite Eq. (43) with observable and density still a function of the initial point x:

$$\int dx\, A^t(x) e^{-\beta A^t(x)} \left[\mathcal{L}_t^\dagger w \right](x) = \int dx\, e^{-\beta A^t(x)} A^t(x) \int dy\, \delta(y - f^t(x)) w(y), \tag{61}$$

The density evolution is then expanded in terms of the eigenspectrum of the Koopman operator $\mathcal{L}_t^\dagger$. As imaginable, the average of A^t is now 'dual' to the expression (49):

$$\langle A^t \rangle_\beta = \frac{\sum_n^\infty \tilde{b}_n e^{-\gamma_n t} \int dx\, \varphi_n(x) A^t(x) e^{-\beta A^t(x)}}{\sum_n^\infty \tilde{b}_n e^{-\gamma_n t} \int dx\, \varphi_n(x) e^{-\beta A^t(x)}}, \tag{62}$$

with

$$\tilde{b}_n = \int dy\, w(y) \phi_n(y). \tag{63}$$

As before with the $\varphi_n(x)$, this time the eigenfunctions $\phi_n(x)$ of the Perron-Frobenius operator are hidden in the coefficients $\tilde{b}_n$ of the expansion, and yet they come out when we take a density pinned at a definite point, $w(x) = \delta(x - x_t)$. Then the average of the integrated observable becomes the distribution

$$\langle A^t \rangle_{\beta=0}(x_t) = \frac{\int dx\, A^t(x) \int dy\, \delta(y - f^t(x)) \delta(y - x_t)}{\int dx \int dy\, \delta(y - f^t(x)) \delta(y - x_t)} = \frac{A^t(f^{-t}(x_t))}{|\det J^t(f^{-t}(x_t))|\, \mu(\mathcal{M}(t))}. \tag{64}$$

Specularly to Eq. (52), we obtain for the distribution $\hat{A}^t(f^{-t}(x_t))$ in terms of the spectral expansion,

$$\hat{A}^t(f^{-t}(x_t)) := \langle A^t \rangle_{\beta=0}(x_t) = \frac{\sum_n^\infty \phi_n(x_t) e^{-\gamma_n t} \int dx\, \varphi_n(x) A^t(x)}{\sum_n^\infty \phi_n(x_t) e^{-\gamma_n t} \int dx\, \varphi_n(x)}. \tag{65}$$

The meaning of the previous expression is that the phase-space distribution of any integrated observable pinned by the *arrival* point x_t in the phase space is a superposition of eigenfunctions of the Perron-Frobenius operator. The truncation (54) may be applied here as well, for timescales of the order $(\gamma_1 - \gamma_0)^{-1}$:

$$\hat{A}^{-t}(x_t) := \frac{A(f^{-t}(x_t))}{\mu(\mathcal{M}(t))|\det J^t(f^{-t}(x_t))|} \simeq \int_\mathcal{M} A^t(x) \varphi_0(x)\, dx + \frac{\phi_1(x_t)}{\phi_0(x_t)} e^{-(\gamma_1 - \gamma_0)t} \int_\mathcal{M} A^t(x) \varphi_1(x)\, dx. \tag{66}$$

D. Evolution on the manifold

An argument was presented in [15, 16] to show that the evolution of a density by the Perron-Frobenius operator along the unstable manifold of an area-preserving, fully chaotic map leads to the following result: the distribution of the finite-time Lyapunov exponents in the phase space (the unit torus) follows the pattern of the second eigenfunction of the Perron-Frobenius operator, at a suitable time scale. The idea is that, on the unstable manifold, the Perron-Frobenius operator acts on a density as

$$\mathcal{L}_t w(x) \sim e^{-t\Lambda(f^{-t}(x),t)} w(x) \,, \tag{67}$$

where the Lyapunov trajectory begins at $f^{-t}(x)$ and runs for time t up to x. On the other hand, as seen, the action of the Perron-Frobenius operator on the same density may be expanded and truncated as (assuming no escape)

$$\mathcal{L}_t w(x) = c_0 + c_1 e^{-\gamma_1 t}\phi_1(x) + O\left(e^{-\gamma_2 t}\right)\,. \tag{68}$$

Along the unstable manifold, the evolution is thus linearized as in Eq. (67), and so it does not depend on $w(x)$, but only on the finite-time Lyapunov exponent $e^{-\Lambda(f^{-t}(x),t)}$, whose distribution should then follow $\phi_1(x)$ at a time scale set by γ_1^{-1}:

$$e^{-t\Lambda(f^{-t}(x),t)} \propto \phi_1(x)e^{-\gamma_1 t}\,, \tag{69}$$

meaning that the second eigenfunction of the Perron-Frobenius operator rules the distribution of the finite-time Lyapunov exponents pinned at the final point of each trajectory. That is consistent with Eq. (66), which generalizes the theory to an arbitrary observable (one would use Eq. (54) when pinning the observable distribution at the initial point of each iterated trajectory, instead).

E. Noise

The finite-time thermodynamic formalism exposed in the previous section may also describe a chaotic system with background noise, whose trajectories are solutions to the Langevin equation

$$\frac{dx}{d\tau} = v(x) + \eta(\tau)\,, \tag{70}$$

with random force $\eta(\tau)$. The integrated observable (42) would now take the form

$$A_{\sigma^2}^t(x_0) = \left\langle \int^t a(f_\eta^\tau(x_0))d\tau \right\rangle_{\sigma^2}\,, \tag{71}$$

where $\langle\cdot\rangle_{\sigma^2}$ denotes an ensemble average over noisy trajectories $f_\eta^t(x)$, with isotropic noise of amplitude $2\sigma^2$. In this setting, phase-space densities are transported by an evolution operator with a noisy kernel, for example the Fokker-Planck operator [17] in discrete time, applied at each iteration:

$$[\mathcal{L}_{\sigma^2} w](x) = \frac{1}{\sqrt{4\pi\sigma^2}} \int dx\, e^{-(y-f^t(x))^2/4\sigma^2} w(x)\,. \tag{72}$$

With that change, the distribution of integrated observables, Eq. (52), would become, in the noisy phase space,

$$\langle A^t \rangle_{\beta=0}(x_0) = \frac{A_{\sigma^2}^t(x_0)}{|\mathcal{M}_{\sigma^2}(t)|} = \frac{\sum_n^\infty \varphi_n(x_0)e^{-\gamma_n t}\int dx\phi_n(x)A_{\sigma^2}^t(x)}{\sum_n^\infty \varphi_n(x_0)e^{-\gamma_n t}}\,. \tag{73}$$

Now ϕ and φ are respectively right and left eigenfunctions of the Fokker-Planck operator (72), that retains the spectral gap of the Perron-Frobenius operator, under the same assumptions as in the deterministic picture.

IV. NUMERICS

The above predictions are now tested on different models of chaos, namely the perturbed cat map, the noisy Hamiltonian Hénon map, and the Ikeda map. The strategy is that to numerically compute the first two eigenfunctions of the Perron-Frobenius and of the Koopman spectrum, and compare their ratio with the distributions of different integrated observables for finite time.

The leading- and subleading eigenfunctions of the Perron-Frobenius/Koopman operator are first computed as follows. The transfer operator is projected onto a finite-dimensional vector space, and thus implemented as a matrix, as it is by now common when solving flow (e. g. Liouville [18]) equations. Previous literature warns us that the choice of the discretization is crucial [19], and may deeply affect the eigenspectrum beyond the leading eigenvalue [20]. It has been established, on the other hand, that nonlinear perturbations to linear maps on a torus increase the robustness of the numerically evaluated spectrum under certain conditions [21]. The simplest discretization scheme is Ulam's method [22], that amounts to subdividing the phase space into N intervals $\mathcal{M}_i$ of equal area. The evolution operator is thus approximated with a $N \times N$ transfer matrix whose entries $\mathbf{L}_{ij}$ are the transition probabilities from $\mathcal{M}_i$ to $\mathcal{M}_j$

$$\mathbf{L}_{ij} = \frac{\mu\left(\mathcal{M}_i \bigcap T_\epsilon(\mathcal{M}_j)\right)}{\mu(\mathcal{M}_i)} \tag{74}$$

in one time step, where μ is the Lebesgue measure. I use a known Monte Carlo method [23] to estimate the nonsymmetric transfer matrix $\mathbf{L}_{ij}$, that consists of iterating random initial conditions from each cell $\mathcal{M}_i$ and counting which fraction lands in each $\mathcal{M}_j$. A thorough study of stability and convergence of discretization algorithms has been reported elsewhere by the author and co-workers [16], among others.

A. Perturbed cat map

The first model is the perturbed cat map $f(x) = T_\epsilon \circ T[x]$, with $x = (q, p)$:

$$T\begin{pmatrix} q \\ p \end{pmatrix} = \begin{pmatrix} 1 & 1 \\ 1 & 2 \end{pmatrix} \begin{pmatrix} q \\ p \end{pmatrix} \mod 1, \tag{75}$$

and

$$T_\epsilon \begin{pmatrix} q \\ p \end{pmatrix} = \begin{pmatrix} q - \epsilon \sin 2\pi p \\ p \end{pmatrix} \mod 1. \tag{76}$$

This system is strongly chaotic and hyperbolic, that is,
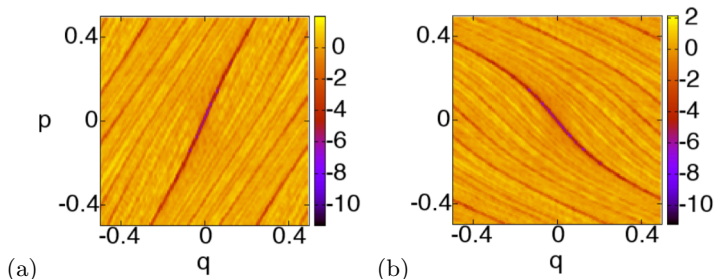
FIG. 1. First subleading eigenfunctions of the (a) Perron-Frobenius- and (b) Koopman operator for the perturbed cat map. The Ulam matrix has size $2^{14} \times 2^{14}$.

correlations decay exponentially fast with time [24]. It possesses an infinite number of unstable periodic orbits, and, specifically, a fixed point at the origin. The phase space is a 2-torus, there is no escape, and areas are preserved by the time evolution, so that the determinant of the Jacobian matrix of every trajectory is equal to unity.

The leading eigenfunctions of the transfer operators for the cat map are uniform distributions, and therefore they will not affect the predictions of the present theory out of equilibrium. Instead, the subleading eigenfunctions of the Perron-Frobenius and Koopman operators, computed with the Ulam method, are shown in Fig. 1.

Here, I first verify prediction (55) for the distribution of an integrated observable pinned by its initial point in the phase space, $A^t(x_0)$. The observables employed here are

1. The finite-time Lyapunov exponent (24) of the cat map.

2. The average diffusion

$$\overline{D}^t(x) = \frac{1}{t} \int_0^t d\tau q^2(f^\tau(x)), \tag{77}$$

with $t \sim \gamma_1^{-1}$.

3. The average kinetic energy

$$\overline{K}^t(x) = \frac{1}{t} \int_0^t d\tau \frac{p^2(f^\tau(x))}{2}, \tag{78}$$

again with $t \sim \gamma_1^{-1}$.

The desired finite-time field distributions are obtained by iterating some 10^8 randomly chosen, uniformly distributed initial conditions until a time t before relaxation. The outcomes are shown in Fig. 2: all the observables are striated along the stable manifold, and, in particular, their distribution profiles are all alike, and their features echo with those of the first subleading eigenfunction of the Koopman operator [Fig. 1(b)]. Enhancement ('scar') of the latter [15] corresponds to suppression ('antiscar') of the integrated observable, which is ascribed to the second term of Eq. (55): it is found that either $\varphi_1(x_0) < 0$ and maximally negative at the scar with the integral $\int dx\, \phi_1(x) A^t(f^{-t})(x)) > 0$ (from numerics), or vice versa [25], and so the pointwise value of the integrated observable $\hat{A}^t$ is approximately given by a constant (its phase-space average) *minus* something proportional to the second eigenfunction of the Koopman operator. As a result, a scar in the second eigenfunction produces an antiscar in the distribution of all integrated observables at time scale γ_1^{-1}, as apparent in all plots of Fig. 2.

Let me now proceed specularly with the validation of the first-order truncation (66) of the expansion (65), for the distribution of an integrated observable pinned by its final point (iteration at time t) in the phase space, $\hat{A}^{-t}(x_t)$. The tested observables are once again the finite-time Lyapunov exponent, the average diffusion, and the kinetic energy. The results are displayed in Fig. 3, and are analogous to what seen with the initial-point pinning, except that all distributions are striated along the unstable manifold of the map, and follow the profile of the second eigenfunction of the Perron-Frobenius operator [Fig. 1(a)], here denoted by $\phi_1(x)$. The equivalence between eigenfunction enhancement and observable suppression is still verified in this case, as one can infer from Eq. (66).

In order to quantify the similarities between the distributions of distinct finite-time observables, Fig. 4 plots the logarithmic ratio

$$r(x_0, t) = \ln \left| \frac{\ln|\Lambda(x_0, t)| - \langle \ln|\lambda(x, t)|\rangle_\mathcal{M}}{\overline{D}(x_0, t) - \langle \overline{D}(x, t)|\rangle_\mathcal{M}} \right| \tag{79}$$

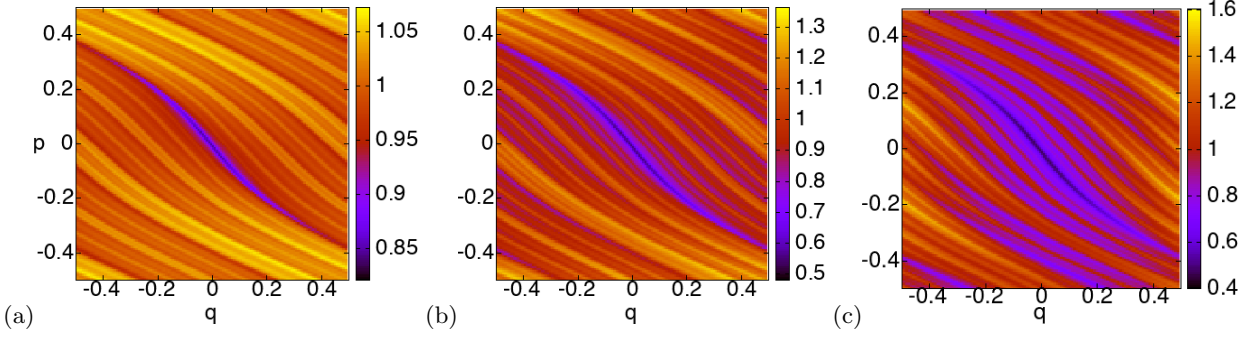between the distributions of the diffusion and the Lyapunov exponent, scaled by their mean values, both in

FIG. 2. The distribution (2^{14} points, each averaged over 10^4 trajectories) of (a) the finite-time Lyapunov exponents, (b) the integrated kinetic energy, (c) the average diffusion, of the perturbed cat map having the (q, p) coordinates as initial points. The map is iterated until time $t = 15$.
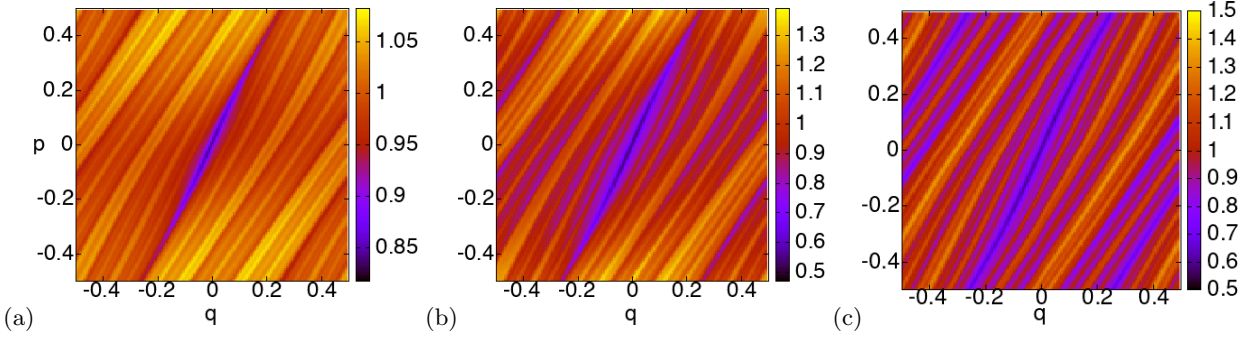

FIG. 3. The distribution (2^{14} points, each averaged over 10^4 trajectories) of (a) the finite-time Lyapunov exponents, (b) the integrated kinetic energy, (c) the average diffusion, of the perturbed cat map having the (q, p) coordinates as final points. The map is iterated until time $t = 15$.

the Perron-Frobenius and in the Koopman pictures of pinpointing. If the present theory holds, we should expect $r(x, t)$ to be a uniform distribution plus or minus fluctuations, and indeed the plots give that indication.
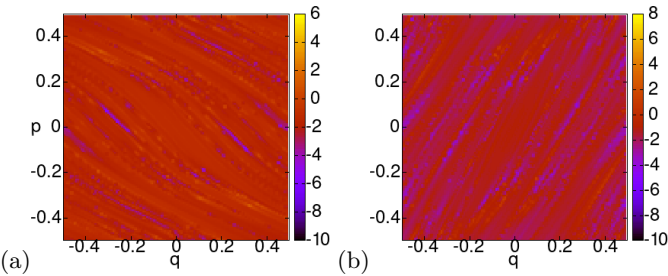

FIG. 4. The logarithmic ratio (79) between the distributions (2^{14} points) of the finite-time Lyapunov exponents to the integrated kinetic energy, for the perturbed cat map having the (q, p) coordinates as (a) initial- and (b) final points. The map is iterated until time $t = 15$.

B. Hamiltonian Hénon map

The next model to test the theory on is the Hamiltonian Hénon map

$$
\begin{aligned}
q' &= 1 - \alpha q^2 + \beta p \\
p' &= p,
\end{aligned}
\tag{80}
$$

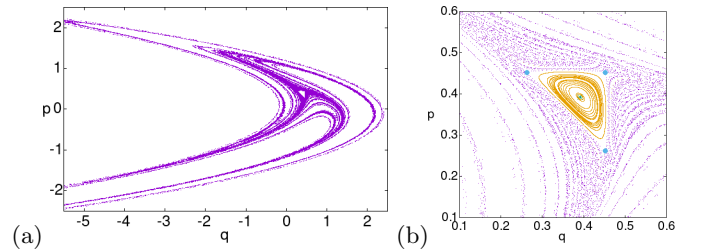with $\alpha = 1.4$ and $\beta = -1$. This map has no dissipation,

FIG. 5. (a) Unstable manifold emanating from the hyperbolic fixed point of the map (80), obtained by forward iteration of 10^6 initial condition until time $t = 15$. (b) Marginally stable fixed point, surrounded by a stability island, triangularly shaped by an outer period-three unstable periodic orbit (blue points).

but it does allow escape to infinity from the neighborhood

of the hyperbolic fixed point $x_p \simeq (-1.1, -1.89)$, that generates a chaotic saddle through its stable and unstable manifolds (the latter is portrayed in Fig. 5(a)). A second fixed point, $x_c \simeq (0.39, 0.39)$, is marginally stable, and surrounded by a small non-hyperbolic region (Fig. 5(b)). In order to 'kick' the dynamics out of the latter non-chaotic region and into the chaotic phase, weak noise is added to the map (80) of an amplitude comparable to the size of the stability island per unit time.

Strictly speaking, the non-hyperbolicity of the resulting noisy system should introduce a continuous component in the spectrum of the transport operators and thus break the assumption of a solely discrete spectrum. However, if we investigate timescales of the order of- or shorter than the inverse escape rate from the region of the chaotic saddle, when the discrete part of the spectrum is dominant, the contribution of the continuous part of the spectrum may be ignored, due to the smallness of the stability island. Unlike for the cat map, the leading eigenfunctions of the transfer operators for the Hamiltonian Hénon map are not uniform distributions (Fig. 6(a-b)), and, due to the finite escape rate, they are conditionally invariant densities. As a consequence, we should expect from the first-order truncations of Eqs. (54) and (66) that the nonequilibrium distributions of integrated observables follow the profile given by the ratio of the first subleading- to the leading eigenfuntion of $\mathcal{L}$ ($\mathcal{L}^\dagger$).

The theoretical predictions are tested for two observables, that is the finite-time Lyapunov exponent, as well as the diffusivity

$$\hat{D}^t(x) = \frac{1}{t} \int_0^t d\tau \left[q^2(f^\tau(x)) + p^2(f^\tau(x)) \right]. \qquad (81)$$

The density plots in Fig. 7 corroborate the expectations for the field distributions of the two integrated observables to be supported on the stable manifold of the map when pinned by the initial points of the iteration $x_0 \to f^t(x_0)$ plus weak noise, and to mimic the density profile of the ratio between the second and the first eigenfunction of the Koopman operator.

On the other hand, the field distributions of the same observables pinned by the final points of each phase-space trajectory $f^{-t}(x_t) \to x_t$ plus weak noise are supported on the unstable manifold of the map (Fig. 8), and behave similarly to the ratio of the second to the first eigenfunction of the Perron-Frobenius operator. In both 'forward' and 'backward' pictures, the strongly chaotic phase (in orange) is distinguishable from the non-hyperbolic, weakly chaotic phase (in blue) of a three-lobed shape with tapered ends, due to a period-three unstable periodic orbit that rules the dynamics just outside the stability island (Fig. 5(b)).

Figures 7(a)-(b) and 8(a)-(b) show that the distributions of the two observables are nearly identical, and their ratio distributions (Figs. 7(d) and 8(d)) are very close to be uniform, except for deviations visible in the non-hyperbolic region of the phase space.

The white color in Figs. 7-8(a)-(b) represents the region of the phase space where forward (Fig. 7) or backward (Fig. 8) trajectories escape from the domain examined before the time t of integration, and thus it is not part of the field distributions. In Figs. 7-8(c), instead, the ratio between the eigenfunctions is not defined in the blank region, where the leading eigenfunction vanishes.

The density plots of the leading- and subleading eigenfunctions of the transport operators (Figs. 7-8(d)-(e)) taken separately, bear significant differences from the fields of the observables: the first eigenfunctions clearly describe a longer timescale than that of the field distributions, at which noisy trajectories have mostly left the hyperbolic region, while they only survive in and around the stability island; the second eigenfunctions alone are more resemblant of the finite-time fields, except they are suppressed on a ring around the stability island, a feature that does not have a kin in the distributions of the observables. Therefore, it does appear as though the finite-time fields distributions are best described by the ratio ϕ_1/ϕ_0 (φ_1/φ_0).

C. Ikeda map

Let me now consider the Ikeda map

$$\begin{aligned} q' &= c_0 + c_2 q \cos\theta - c_2 p \sin\theta \\ p' &= c_2 q \sin\theta + c_2 p \cos\theta \,, \end{aligned} \qquad (82)$$

with $\theta = c_1 - \frac{c_3}{1 + q^2 + p^2}$, while the parameters are set to $c_0 = 1$, $c_1 = 0.4$, $c_2 = 0.9$, $c_3 = 6$. The Ikeda map with these parameters features a strange attractor, that is the closure of the unstable manifold of the fixed point at $x_s \simeq (0.5228, 0.2469)$ (inverse saddle), and whose basin of attraction is bounded by the stable and unstable manifolds of the hyperbolic fixed point $x_h \simeq (1.1142, -2.2857)$ [26].

The Ikeda map is dissipative, and thus it does not preserve areas in the phase space, which are instead shrunk by the evolution. This phenomenon is known as squeezing, and it adds to the stretching and folding already seen in the previous Hamiltonian examples, but now plays a central role.

The first consequence of squeezing would be a strange attractor with a non-smooth measure, that emerges at long times. In order to avoid fractal measures in the phase space, that would prevent the present theory from applying, noise of amplitude $2\sigma^2 = 0.025$ is added to the dynamics (82). Collaterally, some noisy orbits may now cross the stable manifold of the fixed point x_h, and exit the region of the strange attractor, which produces a tiny but non-zero escape rate.

The second effect of squeezing is a complex-conjugate pair of second eigenvalues for the transport operators, instead of the real and isolated single eigenvalue encountered in the previous Hamiltonian models. The second eigenvalue of the Perron-Frobenius operator yields the
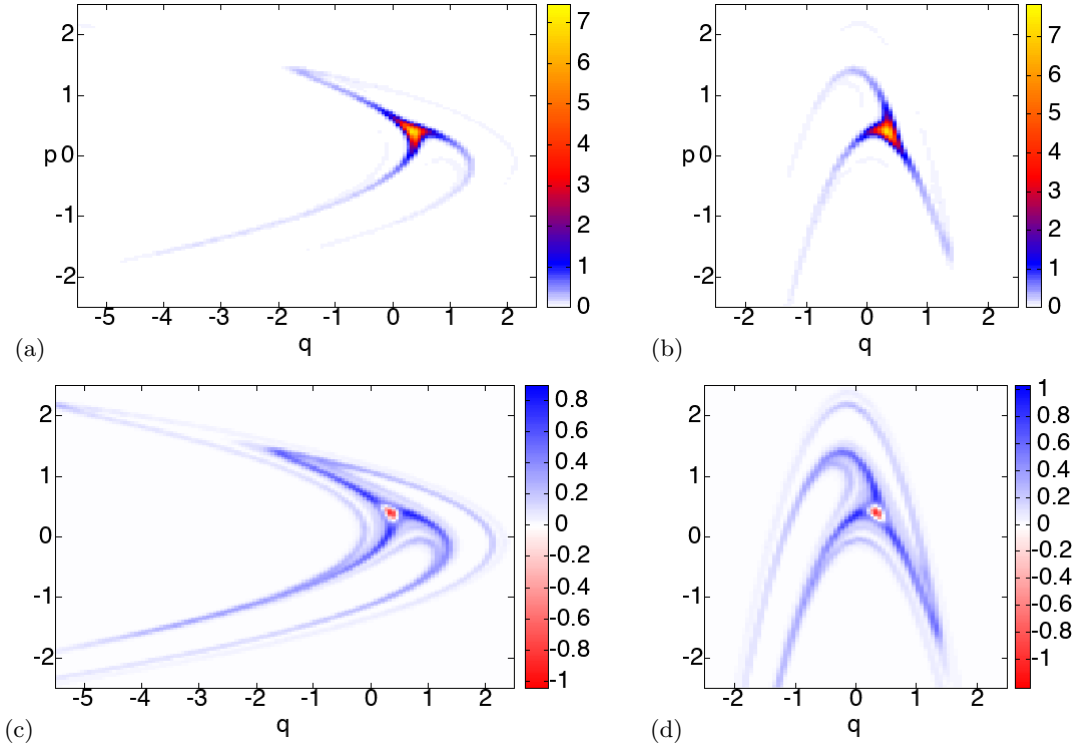
FIG. 6. (a-b): Leading eigenfunctions of the (a) Perron-Frobenius- and (b) Koopman operator for the Hénon map.(c-d): First subleading eigenfunctions of the same operators, respectively. The Ulam matrix has size $2^{14} \times 2^{14}$.
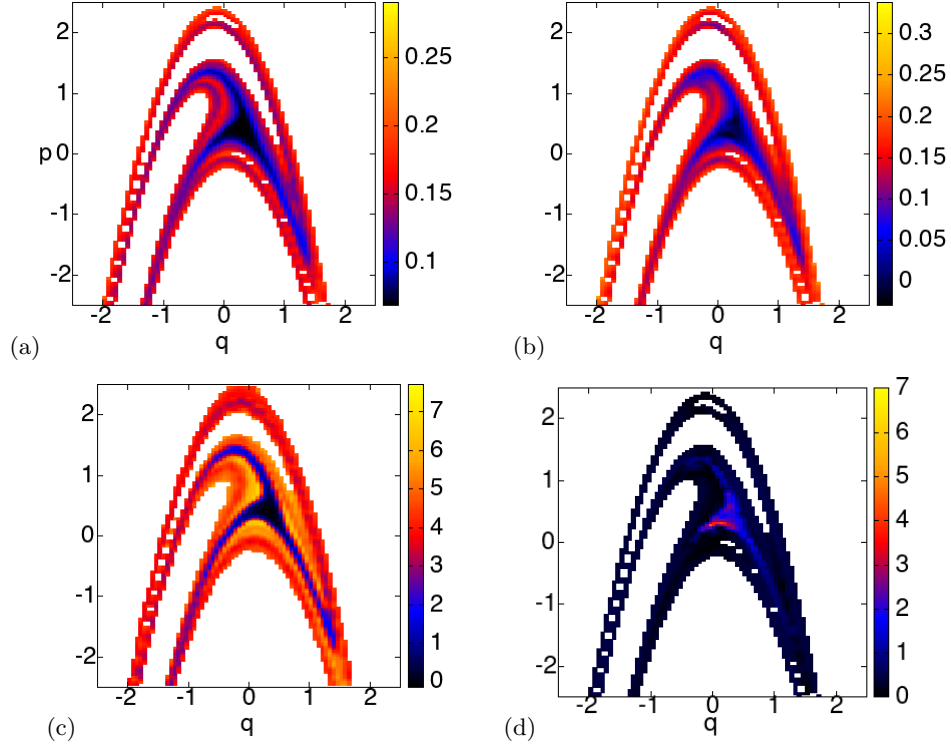

FIG. 7. (a): Phase-space distribution (2^{14} points, each averaged over 10^4 trajectories) of the diffusivity (81) for the Hénon map, pinned by the initial points, after $t = 10$ iterations of the map. (b): Phase-space distribution of the finite-time Lyapunov exponents, $t = 10$. (c) Ratio of the first subleading- to the leading eigenfunction of the Koopman operator for the same map. (d) ratio of the distributions of the observables in (a) and (b), as defined in (79).

decay rate of any initial density to the natural measure   of the phase space, which can be estimated from the au-
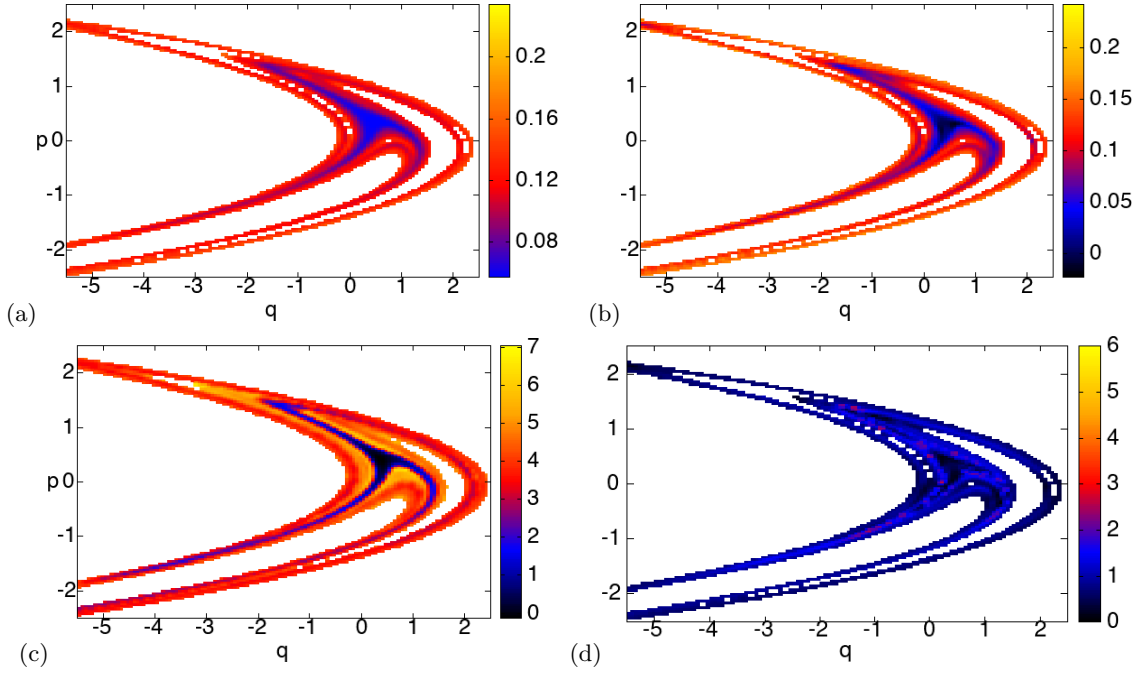
FIG. 8. (a): Phase-space distribution (2^{14} points, each averaged over 10^4 trajectories) of the diffusivity (81) for the Hénon map, pinned by the final points, after $t = 10$ iterations of the map. (b): Distribution of the finite-time Lyapunov exponents, $t = 10$. (c) Ratio of the first subleading- to the leading eigenfunction of the Perron-Frobenius operator for the same map. (d) ratio of the distributions of the observables in (a) and (b), as defined in (79).
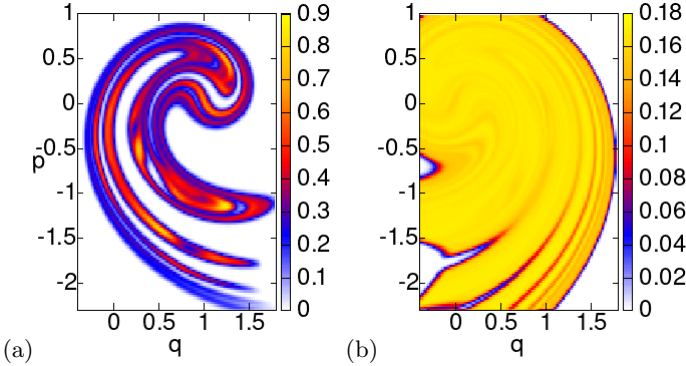

FIG. 9. First eigenfunctions of the (a) Perron-Frobenius- and (b) Koopman operator for the Ikeda map with additive noise of amplitude $\sigma^2 = 2.5 \cdot 10^{-3}$. The Ulam matrix has size $2^{14} \times 2^{14}$.

tocorrelation function

$$C(t) = \frac{\int w(x) \left[\mathcal{L}_t w\right](x)}{\int w^2(x)} . \tag{83}$$

Here $C(t)$ is computed for an initial Gaussian density centered at the fixed point of the map, transported by the Ulam matrix $\mathbf{L}^t$, which approximates $\mathcal{L}_t$, and plot it as a function of time in Fig. 10(f), where it can be clearly seen to oscillate while decaying. A non-trivial imaginary part of the first subleading eigenvalue of the Perron-Frobenius/Koopman operator signals oscillations in the decay of correlations, produced by the alternate

effects of stretching, folding, and especially squeezing (Figs. 10(a)-(e)) that creates accumulation regions, unlike in the previous Hamiltonian models, where correlations decay monotonically (Fig. 10(f)).

With that observation, let us look once more at the first non-trivial term in the expansion (54) of the integrated observable $A^t(x_0)$:

$$\varphi_1(x_0)e^{-\gamma_1 t} \int dx \, \phi_1(x)A^t(f^{-t}(x)) \tag{84}$$

is now made of three complex factors, and adds up to a real number with the mirror term of $\varphi_1^*(x_0)$ and $\phi_1^*(x_0)$. In that process, the combination of $\varphi_1(x_0)$ and $\varphi_1^*(x_0)$ gets to depend on $\int dx \, \phi_1(x)A^t(f^{-t}(x))$ and its complex conjugate, which are observable specific. That in fact determines the breakdown of the universal behavior of the finite-time integrated observable distributions predicted by the theory and observed in the previous models. For the Ikeda map, one should not expect the distributions of distinct observables to share the same profile, as they are supposed to follow different linear combinations of the real and imaginary parts of the first subleading eigenfunctions (divided by the natural measure), all observable dependent.

In order to verify that, the plots in Figs. 11(a)-(b) and 12(a)-(b) compare the field distributions of two distinct integrated observables, that is the diffusivity $\hat{D}^t(x)$ defined as in Eq. (81), and the finite time Lyapunov exponent, defined in Eq. (24). This time the directly computed distributions of the two observables are similarly
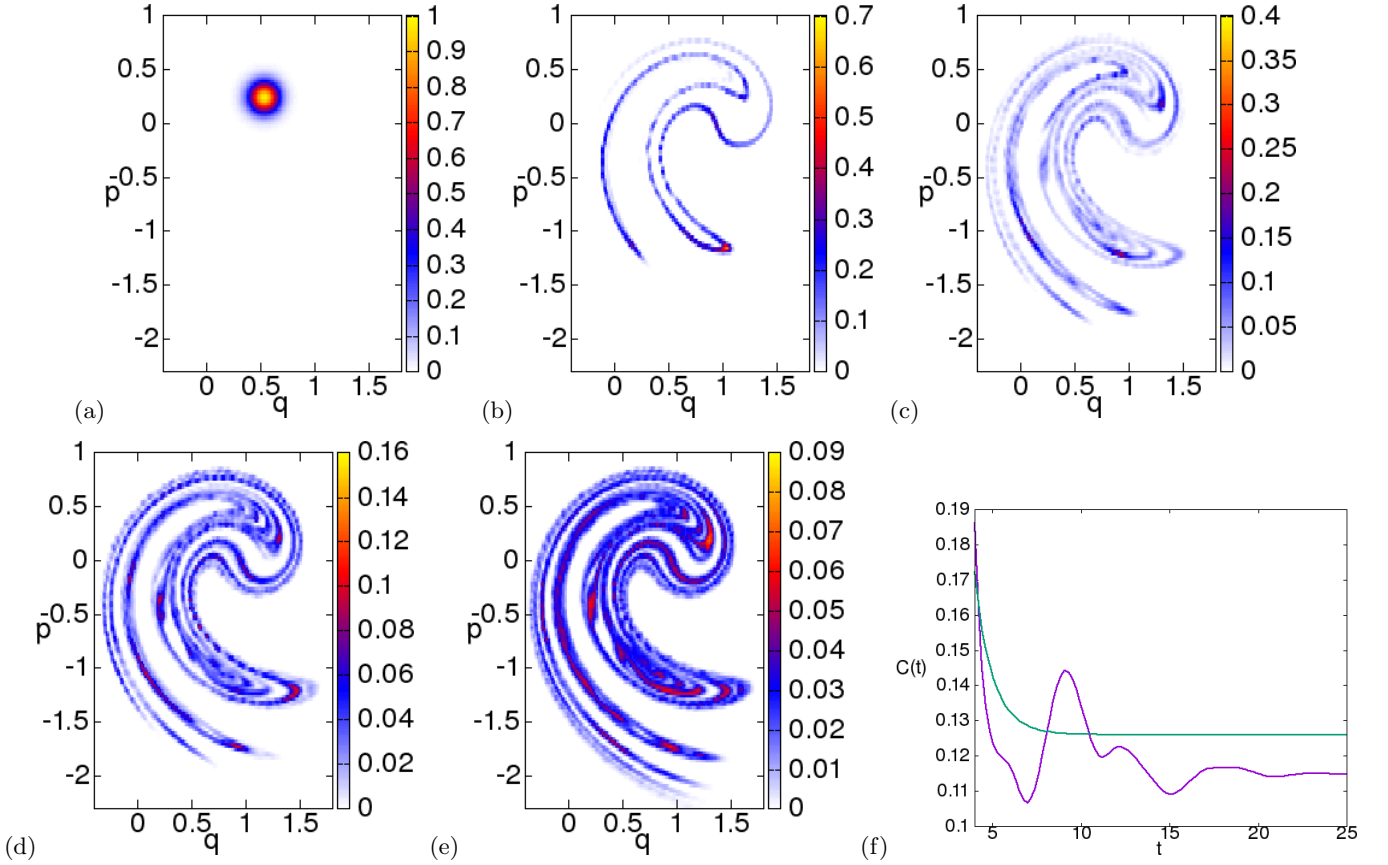
FIG. 10. Snapshots of the evolution of the initial Gaussian density centered at the fixed point $x_s \simeq (0.533, 0.247)$, portayed in (a), by the Ulam matrix of the Ikeda map with noise of amplitude $\sigma^2 = 4 \cdot 10^{-4}$, given by the resolution; (b) $t = 5$; (c) $t = 9$; (d) $t = 11$; (e) $t = 25$. (f) (purple) autocorrelation function of the initial density in (a) with the iterates at an intermediate timescale; (green) autocorrelation function of a density initially centered at the fixed point of the perturbed cat map, for comparison. The Ulam matrix has size $2^{12} \times 2^{12}$.

supported on and striated along the unstable (Fig. 11) and stable (Fig. 12) manifolds respectively, but their profiles share limited similarities.

In particular, certain features that belong now to the real- now to the imaginary part of the second eigenfunction (divided by the first, that is real valued, Figs. 11(d)-(e) and 12(d)-(e)) may be visible in the profiles of either observable distribution (Figs. 11(a)-(b) and 12(a)-(b)), but not in a consistent manner, as seen for the non-dissipative models of the previous sections.

The ratios $r(x, t)$, as defined in (79), between the distributions of the two integrated observables (Figs. 11(c) and 12(c)) are also striated along the manifolds, meaning that they are no longer uniform distributions with fluctuations. That indeed gives an additional indication that distinct integrated observables produce different finite-time field distributions.

V. SUMMARY

I have carried out an attempt to take the thermodynamic formalism of chaotic dynamics out of statistical equilibrium. The time evolution of the phase space is treated as a thermodynamic ensemble, and the single chaotic trajectories as its susbsystems. The probability for the value of a given observable on a trajectory follows the usual Gibbs expression, but now it depends on the time-dependent statistical weight of each orbit.

With those premises, the familiar expressions relating Rényi (e. g. information) entropy, a free energy ('topological pressure'), and ensemble averages, are extended to chaotic processes that have yet to relax to statistical equilibrium.

The most notable byproduct of the present construction emerges from the evaluation of the ensemble average of an integrated observable. According to the theory, every such expectation value does depend explicitly on a phase-space weight distribution, which in turn depends both on time and, crucially, on the initial conditions. That makes average and higher moments not so meaningful by themselves, and so one rather studies the behavior of the full field distributions of an integrated observable, whose profiles are found to be determined by the first two eigenfunctions of the transport (Perron-Frobenius or Koopman) operator, at an intermediate timescale dur-
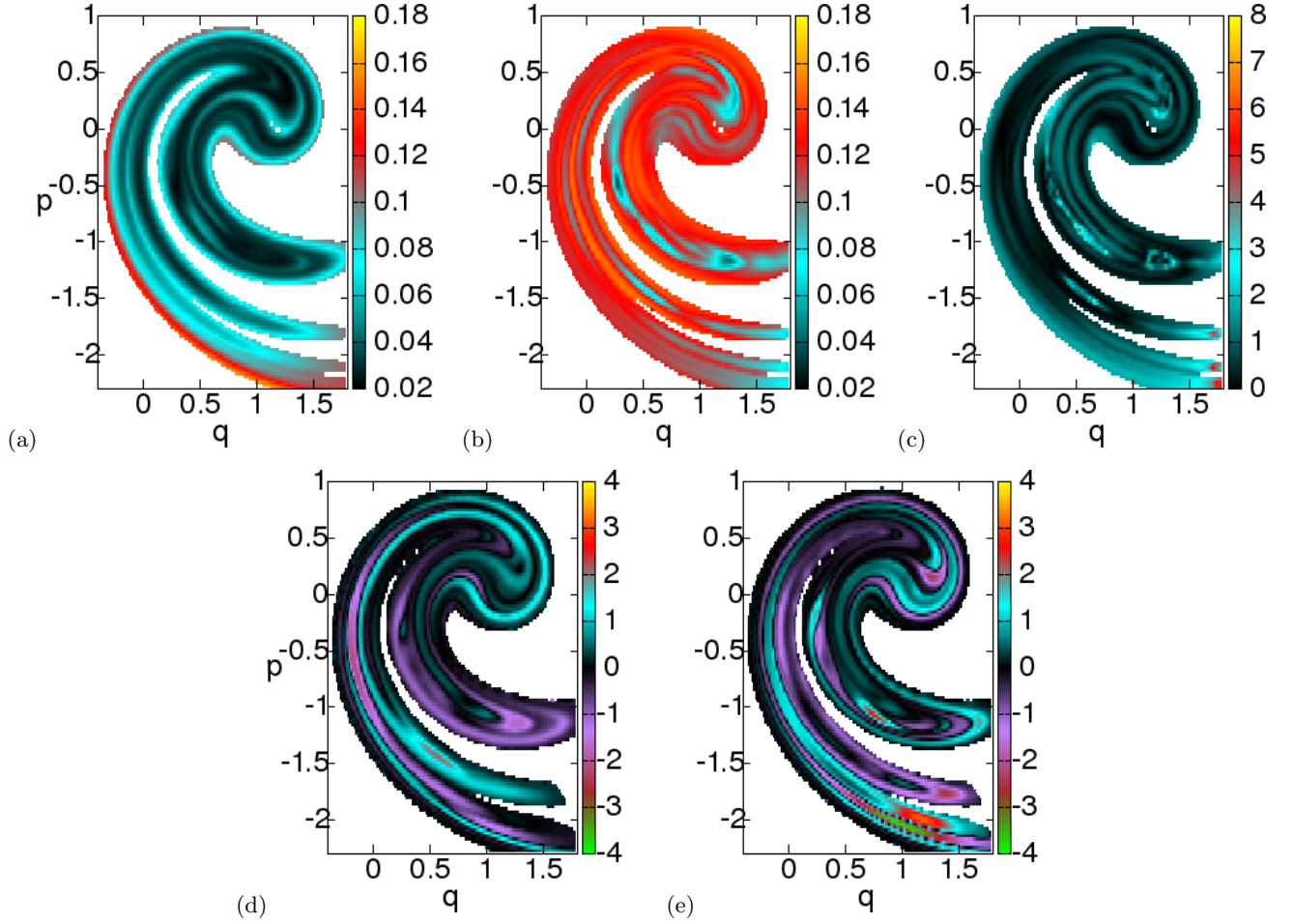
FIG. 11. (a): Distribution (2^{14} points, each averaged over 10^4 trajectories) of the diffusivity for the Ikeda map with noise of amplitude $2\sigma^2 = 2.5 \cdot 10^{-3}$, pinned by the final points, after $t = 8$ iterations of the map. (b): Distribution of the finite-time Lyapunov exponents, $t = 8$. (c): Ratio of (b) to (a), as defined in (79). (d)-(e): Real- and imaginary parts respectively of the second eigenfunction of the Perron-Frobenius operator, divided by the first eigenfunction.

ing relaxation. This outcome, and the prediction of an observable-independent behavior for the profile distributions, is obtained with an alternative approach to that of dynamical averages, used for both pointwise- and integrated observables in a recent report [27], and thus independently confirms the conclusions of that work.

However, the present results are subject to a number of assumptions, and thus limitations. First, the dynamics must allow for a transport operator with a discrete spectrum, and a spectral gap. Typically, that occurs with a strongly chaotic ('hyperbolic') phase space, or, as seen for the Hamiltonian Hénon map, a chaotic repeller bearing a small stability island, and an appropriate choice of the functional space. Secondly, the universality of the observable field distributions breaks down when the second eigenvalue of the transport operator is a complex conjugate pair instead of a real-valued singlet. This is ascribed to the phase-space squeezing caused by dissipa-

tion, manifest for example in strange attractors.

The present approach to finite-time thermodynamic formalism proves self-consistent when I formally identify the weights of the out-of-equilibrium Gibbs probabilities with phase-space densities, which are pushed forward or pulled back by well-known transport operators. Then, physically meaningful expressions for the ensemble averages are recovered. Moreover, the consequent analysis of finite-time field distributions is corroborated by numerics. Yet, I did not provide a mathematically rigorous theory akin to that already existing for chaotic systems at statistical equilibrium, where, for instance, it is proved that the conventional Gibbs probabilities extremize the topological entropy. Future developments of this line of research should also move in that direction, possibly leveraging variational principles for systems out of equilibrium, such as Maximum Caliber [28].
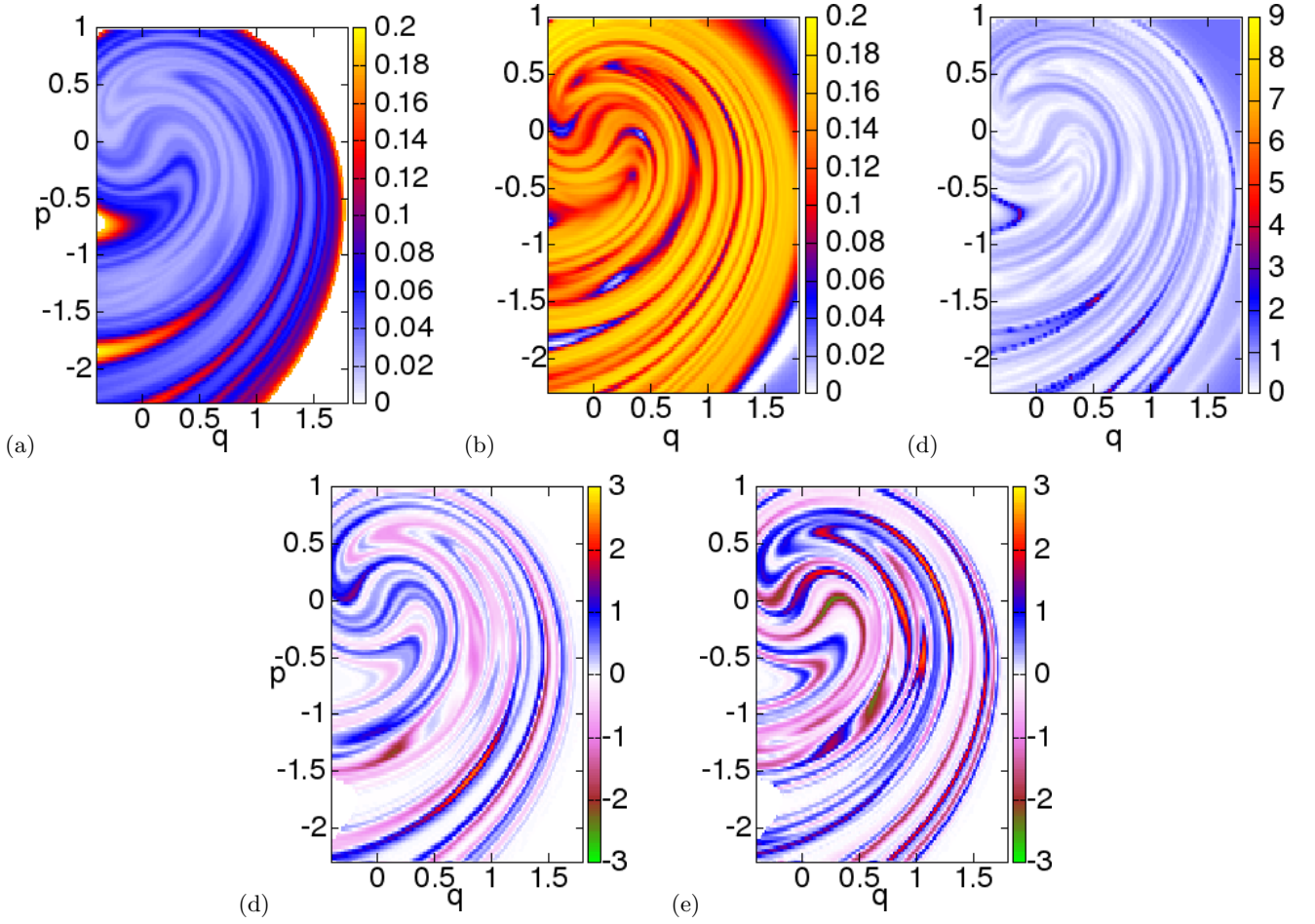
FIG. 12. (a): Distribution (2^{14} points, each averaged over 10^4 trajectories) of the diffusivity for the Ikeda map with noise, pinned by the initial points, after $t = 8$ iterations of the map. (b): Distribution of the finite-time Lyapunov exponents, $t = 8$. (c): Ratio of (b) to (a) , as defined in (79). (d)-(e): Real- and imaginary parts respectively of the second eigenfunction of the Koopman operator, divided by the first eigenfunction.

[1] R. Bowen, *Equilibrium States and the Ergodic Theory of Anosov Diffeomorphisms*, Springer, 1975.

[2] C. Beck and F. Schlögl, *Thermodynamics of Chaotic Systems*, Cambridge, 1997.

[3] P. Gaspard, *Chaos, Scattering, and Statistical Mechanics*, Cambridge, 1998.

[4] D. Ruelle, *Thermodynamic Formalism: The Mathematical Structure of Equilibrium Statistical Mechanics*, Cambridge, 2004.

[5] P. Cvitanović, R. Artuso, R. Mainieri, G. Tanner and G. Vattay, *Chaos: Classical and Quantum*, ChaosBook.org (Niels Bohr Institute, Copenhagen 2020).

[6] J. Slipantschuk, O. F. Bandtlow, and W. Just, Symmetry decomposition of chaotic dynamics, J. Phys. A: Math. Theor. **46**, 075101 (2013).

[7] N. R. Smith, Large deviations in chaotic systems: exact results in dynamical phase transitions, Phys. Rev. E **106**, L042202 (2022).

[8] H. Kantz and P. Grassberger, Repellers, semi-attractors, and long-lived chaotic transients, Physica D **17**, 75

(1985).

[9] According to reference [2], the quantity to be minimized is the function $\Psi_t(a, p) = \sum_j p_j \beta E_j + p_j \ln p_j$.

[10] J. P. Eckmann and D. Ruelle, Ergodic theory of chaos and strange attractors, Rev. Mod. Phys. **57**, 617.

[11] R. Chetrite and H. Touchette, Nonequilibrium microcanonical and canonical ensembles and their equivalence, Phys. Rev. Lett. **111**, 120601 (2013).

[12] R. Chetrite and H. Touchette, Nonequilibrium Markov processes conditioned on large deviations, Ann. Henri Poincaré **16**, 2005 (2015).

[13] I assume the flow f^t to be invertible, so there is a $1 - 1$ correspondence between every x and $f^{-t}(x)$.

[14] A. Lasota and M. MacKey, *Chaos, Fractals, and Noise; Stochastic Aspects of Dynamics*, Springer, New York, 1994.

[15] D. Lippolis, A. Shudo, K. Yoshida, and H. Yoshino, Scarring in classical chaotic dynamics with noise, Phys. Rev. E **103**, L050202 (2021).

[16] K. Yoshida, and H. Yoshino, A. Shudo, and D. Lippo-

lis, Eigenfunctions of the Perron-Frobenius operator and the finite-time Lyapunov exponents in uniformly hyperbolic area-preserving maps, J. Phys. A: Math. Theor. **54**, 285701 (2021).

[17] P. Cvitanović and D. Lippolis, Knowing when to stop: How noise frees us from determinism, AIP Conf. Proc. **1468**, 82 (2012).

[18] D. J. Chappell and G. Tanner, Solving the stationary Liouville equation via a boundary element method, J. Comp. Phys. **234**, 487 (2013).

[19] G. Froyland, On Ulam approximation of the isolated spectrum and eigenfunctions of hyperbolic maps, Discr. Cont. Dyn. Syst. **17**, 671 (2007).

[20] F. Brini, S. Siboni, G. Turchetti, and S. Vaienti, Decay of correlations for the automorphism of the torus $\mathbb{T}^2$, Nonlinearity **10**, 1257 (1997).

[21] M. Blank, G. Keller, and C. Liverani, Ruelle-Perron-Frobenius spectrum for Anosov maps, Nonlinearity **15**, 1905 (2002).

[22] S. M. Ulam, *A Collection of Mathematical Problems* (Interscience, New York, 1960).

[23] L. Ermann and D. L. Shepelyansky, The Arnold cat map, the Ulam method, and time reversal, Physica D **241**, 514 (2012).

[24] V. I. Arnold and A. Avez, *Erogdic Problems of Classical Mechanics*, Benjiamin, New York, 1968.

[25] Here the evolution operators are approximated with matrices, meaning that the numerically computed normalized eigenvectors are determined up to a sign. In any case the φ_n must be bi-orthogonal to the ϕ_n, while the $A^t(f^{-t}(x))$ considered here are positive definite, hence the sign of φ_n determines the sign of the integral $\int dx\, \phi_n(x) A^t(f^{-t}(x))$ as well.

[26] G. Osipenko, *Dynamical Systems, Graphs, and Algorithms*, Springer, 2007.

[27] D. Lippolis, Chaotic fields behave universally out of equilibrium, arXiv:2402.11976 .

[28] P. D. Dixit, J. Wagoner, C. Weistuch, S. Pressé, K. Ghosh and K. A. Dill, Maximum caliber is a general variational principle for dynamical systems, J. Chem. Phys. **148**, 010901 (2018).